INSTITUTE OF PHYSICS PUBLISHING JOURNAL OF PHYSICS D: APPLIED PHYSICS

J. Phys. D: Appl. Phys. **37** (2004) 318–325 PII: S0022-3727(04)67684-4

The dielectric properties of charged nanoparticle colloids at radio and microwave frequencies

Shahid Hussain[1], **Ian J Youngs**[1] **and Ian J Ford**[2]

[1] Future Systems Technology Division, QinetiQ Limited, Cody Technology Park, Farnborough, Hampshire, GU14 0LX, UK

[2] Department of Physics and Astronomy, University College London, Gower Street, London, WC1E 6BT, UK

Received 19 August 2003
Published 14 January 2004
Online at stacks.iop.org/JPhysD/37/318 (DOI: 10.1088/0022-3727/37/3/002)

Abstract

Charged particle colloids typically consist of particles with negative surface charge suspended in an aqueous electrolyte solution. A layer of ions forms around each particle, and previous research has shown that the dynamics of this charge distribution, induced by an external field, lead to effective and potentially useful dielectric properties (Lyklema J and Van Leeuwen H P 1999 *Adv. Colloid and Interface Sci.* **83** 33, O'Konski C T 1960 *J. Phys. Chem.* **64** 605). Charged nanoparticle colloids are potentially of great benefit because they are extremely stable and their small dimensions make them highly versatile. Possible uses include electromagnetic shielding devices and medical applications. This research focuses on the dielectric properties of charged polystyrene nanoparticle colloids, which are investigated across a range of radio and microwave frequencies. The results show two distinct regions in the permittivity behaviour. The first is the dipolar relaxation of water at microwave frequencies. The second is a high amplitude, low frequency relaxation due to the diffusive motion of ions in the bulk electrolyte beyond the double layer. Effective control of the resulting dielectric response is demonstrated with particle size ranging from 20 to 220 nm. It is shown that the small nanoparticle sizes lead to faster relaxation times than those expected from conventional micron particle sizes, such that the loss extends to microwave frequencies. The results are fitted to a model where the zeta potential, ξ, and double layer thickness, κ^{-1}, are used as fitting parameters.

1. Introduction

Charged particle colloids have been the focus of research for many years [1–4]. The dynamics of the charge distributions within these systems lead to interesting dielectric properties, which occur over a range of timescales determined by various aspects of the system. The motivation of our work stems from the need to explore systems exhibiting losses at microwave frequencies. The properties of charged colloids have been extensively studied at radio frequencies, but very little attention has been given to their properties at microwave frequencies. This is likely to be due to the fact that the charge dynamics within the systems studied to date, with particles several micrometres in diameter, are too slow to exhibit significant loss at microwave frequencies. By reducing the size of the colloid particles, however, it should be possible to accelerate the charge dynamics and extend control over the dielectric properties into the microwave region. We have therefore studied nanoparticle colloids.

Section 2 discusses the fundamental properties of charged colloids and describes a model to determine the resulting dielectric properties. Section 3 describes the experimental details. The results obtained are summarized in section 4 and compared with the model. The conclusions arising from the research are discussed in section 5.

2. Mechanisms responsible for the dielectric properties of charged particle colloids

This section describes some of the charge dynamics that lead to the dielectric properties exhibited by charged particle colloids. These are extensively discussed elsewhere [1] and so will only be summarized here in the context of the research undertaken.

The response of the colloids to an applied field is discussed here in terms of the complex dielectric constant or effective permittivity:

$$\varepsilon(\omega) = \varepsilon'(\omega) - \mathrm{i} \cdot \varepsilon''(\omega), \tag{1}$$

where ε' and ε'' are the real (energy storage) and imaginary (energy loss) components of the effective permittivity, respectively, and ω is the angular frequency.

Charged particle colloids typically consist of polystyrene particles with negative charge suspended in an aqueous electrolyte solution. When such a particle is placed in an aqueous environment, its negative surface charge attracts counterions, which leads to the formation of a double layer of charge. The motion of the two types of ions from the bulk electrolyte when driven by an external oscillating electric field will therefore be different.

In the absence of an applied electric field, the equilibrium electrostatic potential, ϕ, is related to the charge density, $\rho(\boldsymbol{r})$, via Poisson's equation:

$$\nabla^2\phi = -\frac{\rho(\boldsymbol{r})}{\varepsilon}, \tag{2}$$

where the permittivity $\varepsilon = \varepsilon_\mathrm{r}\varepsilon_0$ and the charge density is given by

$$\rho(r) = e(n^+(\boldsymbol{r}) - n^-(\boldsymbol{r})), \tag{3}$$

where $n^+(\boldsymbol{r})$ and $n^-(\boldsymbol{r})$ represent the positive and negative ion densities and e is the elementary charge.

The positive and negative ion densities are related to the electrostatic potential via Boltzmann's distribution:

$$n^\pm(\boldsymbol{r}) = n_0^\pm \exp\left(\frac{\pm e\phi(\boldsymbol{r})}{kT}\right), \tag{4}$$

where n_0^+ and n_0^- are the equilibrium positive and negative ion densities, k is Boltzmann's constant and T is the temperature.

The equilibrium electrostatic potential is then calculated by solving the resulting Poisson–Boltzmann equation [5], corresponding to zero total current density, $\boldsymbol{j}^\pm$, from diffusive and field induced motion of the positive and negative ions:

$$\boldsymbol{j}^\pm = \pm n^\pm(\boldsymbol{r})u\nabla\phi - D\nabla n^\pm(\boldsymbol{r}), \tag{5}$$

where u is the mobility and D is the diffusion coefficient of the ions.

Now, when a time varying electric field ($\boldsymbol{E} = \boldsymbol{E}_0\mathrm{e}^{\mathrm{i}\omega t}$) is applied to a charged polystyrene particle, the tangential component of the electric field around the particle surface causes azimuthal transport of the double layer ions across the particle. This results in an asymmetric charge distribution in the double layer around the particle (as shown in figure 1). The charge redistribution is accompanied by a change in dipole strength. This gives rise to a resultant electric field, $\delta\boldsymbol{E}$, around the particle, which opposes the applied field as shown in figure 1. The field, $\delta\boldsymbol{E}$, has components tangential and perpendicular to the particle surface [6]. Therefore, the external field-driven charge redistribution will take place tangential and perpendicular to the particle surface, which leads to a number of relaxation, or energy dissipating, mechanisms [1].

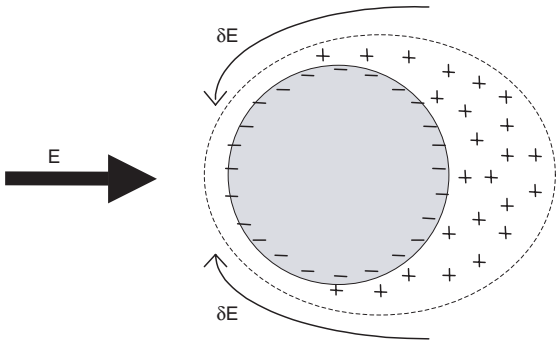

Figure 1. The charge redistribution resulting from the applied field, $\boldsymbol{E}$. The change in dipole strength gives rise to a resultant electric field, $\delta\boldsymbol{E}$.

O'Brien [6] showed that the tangential and perpendicular flow of counterions in the double layer result in a high frequency, low amplitude relaxation (i.e. low energy dissipation), with the relaxation time, τ_1, given by

$$\tau_1 \approx \frac{1}{\kappa^2 D}, \tag{6}$$

where κ is the reciprocal of the double layer thickness and D is the ion diffusivity [5, 7].

After this rapid change in the charge density of the double layer, a slower, low frequency, high amplitude relaxation takes place within the electrolyte, resulting from the changes in the dipole strength of the double layer. The low frequency relaxation time, τ_2, associated with this process is given by

$$\tau_2 = \frac{R^2}{D}, \tag{7}$$

where R is the radius of the particle. The size dependence of this dissipative process is of particular interest here.

2.1. Modelling the dielectric properties

The dielectric dispersion (i.e. frequency dependence of the permittivity) associated with the charge dynamics can be determined by considering the change in electrostatic potential, $\delta\phi$, and ion densities, $\delta n^\pm$, resulting from an applied field, which can be represented as

$$\phi \to \phi + \delta\phi, \tag{8}$$

$$n^\pm \to n^\pm + \delta n^\pm. \tag{9}$$

The continuity of ions is given by

$$\nabla \cdot \boldsymbol{j}^\pm + \frac{\partial \delta n^\pm}{\partial t} = 0, \tag{10}$$

which leads to two boundary conditions:

$$\nabla \cdot \boldsymbol{j}^+ + \nabla \cdot \boldsymbol{j}^- = -\mathrm{i}\omega(\delta n^+ + \delta n^-), \tag{11}$$

$$\nabla \cdot \boldsymbol{j}^+ - \nabla \cdot \boldsymbol{j}^- = -\mathrm{i}\omega(\delta n^+ - \delta n^-). \tag{12}$$

The change in electrostatic potential, $\delta\phi$, and ion densities, $\delta n^{\pm}$, can then be calculated by solving these equations, together with equation (5). Such a solution is obtained by Chassagne and Bedeaux [5], where additional boundary conditions associated with the fields, densities and ion fluxes describing the double layer and the behaviour of the bulk electrolyte far from the particle (asymptotic behaviour) are used. This can then be used to derive an expression for the dipolar coefficient, $\beta(\omega)$. The relationship between $\beta(\omega)$ and permittivity will be given shortly. The model of Chassagne and Bedeaux is valid for all double layer thicknesses, κ^{-1}, and zeta potentials, ξ (related to the electrostatic potential of the double layer [8]). The result derived by Chassagne and Bedeaux for the high zeta potential case is presented here (equation (13)). A more detailed description of the parameters used to model this behaviour can be found in [5].

$$\beta(\omega) = \frac{K_2 - K_1 + 2K_{\parallel}^{\mathrm{s}}/R + K_{\perp}^{\mathrm{D}}/R}{K_2 + 2K_1 + 2K_{\parallel}^{\mathrm{s}}/R - 2K_{\perp}^{\mathrm{D}}/R}, \tag{13}$$

where K_1 and K_2 are the electrolyte and particle complex conductances, respectively, $K_{\parallel}^{\mathrm{s}}$ represents the complex conductance of the double layer along the particle surface and $K_{\perp}^{\mathrm{D}}$ is the perpendicular complex conductance due to the diffusion layer outside the double layer. $K_{||}^{\mathrm{s}}$ and $K_{\perp}^{\mathrm{D}}$ are both related to the zeta potential, as shown by equations (14) and (15) [8].

$$K_{\parallel}^{\mathrm{s}} = \frac{-eD}{kT}\left[\left|\frac{q^{\mathrm{s}}\varepsilon_0\varepsilon_1\xi}{R}\right|\right], \tag{14}$$

$$K_{\perp}^{\mathrm{D}} = 2\frac{J_1}{J_2}\frac{eD}{kT}\left[\left|\frac{q^{\mathrm{s}}\varepsilon_0\varepsilon_1\xi}{R}\right|\right], \tag{15}$$

where ε_1 is the electrolyte permittivity, q^{s} is the surface charge density [8] and

$$J_1 = 1 + \lambda_{\mathrm{n}}R, \tag{16}$$

$$J_2 = 2 + 2\lambda_{\mathrm{n}}R + \lambda_{\mathrm{n}}^2R^2 \tag{17}$$

and λ_{n}^2 is an eigenvalue of a matrix equation describing the behaviour beyond the double layer, as summarized by Chassagne and Saville [8].

The dielectric properties of a colloid can be represented by the complex electric conductivity, $K^*(\omega)$:

$$K^*(\omega) = \sigma(\omega) + \mathrm{i}\omega\varepsilon_0\varepsilon'(\omega), \tag{18}$$

where $\sigma(\omega)$ is the frequency dependent conductivity and $\varepsilon'(\omega)$ is the real permittivity of the colloid.

The dipolar coefficient and complex conductivity are related by the Maxwell–Wagner equation [5]:

$$\frac{K^*(\omega) - K_1}{K^*(\omega) + 2K_1} = V\beta, \tag{19}$$

which, at dilute concentrations, reduces to

$$K^*(\omega) = K_1(1 + 3V\beta). \tag{20}$$

The dipolar coefficient and the permittivity of the charged particle colloids can therefore be related by

$$\frac{\varepsilon'(\omega) - \varepsilon_2}{3V\varepsilon_2} = \beta'(\omega) + \frac{\beta''(\omega)K_1}{\omega\varepsilon_0\varepsilon_1}, \tag{21}$$

$$\frac{\varepsilon''(\omega)}{3V\varepsilon_2} = \frac{(\beta'(\omega) - \beta'(0))K_1}{\omega\varepsilon_0\varepsilon_1} - \beta''(\omega), \tag{22}$$

where ε_1 and ε_2 are the electrolyte and particle permittivity, respectively, V is the volume fraction of the particles, β' and β'' are the real and imaginary components of the dipolar coefficient, respectively, and $\varepsilon''(\omega)$ is the imaginary permittivity of the colloid.

Equations (21) and (22) now enable the dielectric properties to be determined using the zeta potential, ξ, and double layer thickness, κ^{-1}, as fitting parameters. An estimate of ξ and κ^{-1} can also be obtained from equations given in [7, 9]. However, equations (21) and (22) are only valid for frequencies much lower than the relaxation frequency of water [10]. They also do not account for the high frequency relaxation region. This is because the model of Chassagne and Bedeaux is valid for frequencies such that $\omega \ll D_{\pm}\kappa^2$, which (as shown by equation (6)), is lower than the high frequency relaxation region. The permittivity calculated using equations (21) and (22) will therefore be referred to as $\varepsilon_{\mathrm{LF}}(\omega)$ in this paper (i.e. substituting $\varepsilon(\omega)_{\mathrm{LF}}$ for $\varepsilon(\omega)$) to represent the low frequency contribution. The contribution from the high frequency relaxation can be accounted for by using a method employed by Grosse and Barchini [11]. Here, the different relaxation regions are represented by a series of Debye type contributions, the sum of which provides the overall contribution to permittivity. The high frequency relaxation parameters are derived using the simplification that the double layer forms a thin conducting shell. This assumption means that the high frequency relaxation mechanism can be modelled as a Maxwell–Wagner process, where it is assumed that the conducting shell provides the contribution to interfacial polarization. The method used by Grosse and Barchini results in a high frequency relaxation amplitude, G_{H} (equation (23)), and time, τ_{H} (equation (24)):

$$G_{\mathrm{H}} = \frac{9V\varepsilon_1(1-V)[(2\sigma_{\mathrm{s}}/RK_1) - (\varepsilon_2/\varepsilon_1)]^2}{[(1-V)(\varepsilon_2/\varepsilon_1) + 2 + V][(1-V)(2\sigma_{\mathrm{s}}/RK_1) + 2 + V]^2}, \tag{23}$$

$$\tau_{\mathrm{H}} = \frac{\varepsilon_0\varepsilon_1[(1-V)(\varepsilon_2/\varepsilon_1) + 2 + V]}{K_1[(1-V)(2\sigma_{\mathrm{s}}/K_1) + 2 + V]}, \tag{24}$$

where σ_{s} is the surface conductivity of the particle, which can be determined from the zeta potential [5, 7].

The additional contribution from water can be determined from the Debye model of relaxation [10, 11]. Here, it is assumed that water undergoes a dipolar relaxation due to a reorientational polarization. The actual relaxation time, τ_{w}, is dependent upon the viscosity of water, η, and the radius, a, of a water molecule:

$$\tau_{\mathrm{w}} = \frac{4\pi a^3\eta}{kT}. \tag{25}$$

For water, $\eta = 10^{-3}\,\mathrm{N\,s\,m^{-3}}$ and $a = 0.14\,\mathrm{nm}$ [10].

Equation (25) can then be used to determine the permittivity contribution, ε_{w}, due to the relaxation of water:

$$\varepsilon_{\mathrm{w}} = n^2 + \frac{\varepsilon_1 - n^2}{1 + \mathrm{i}\omega\tau_{\mathrm{w}}}, \tag{26}$$

where n is the refractive index and $n^2 = 1.7$ for water [10]. In the case of charged particle colloids, the response of water, given by equation (26), is further modified to account for the additional polystyrene particles. This can be accounted for via effective medium theories [12], such as the Looyenga equation given by

$$\varepsilon_{\mathrm{wp}} = [\varepsilon_{\mathrm{w}}^{1/3} + V(\varepsilon_2^{1/3} - \varepsilon_{\mathrm{w}}^{1/3})]^3, \tag{27}$$

where ε_{wp} is the modified response of water in the presence of polystyrene particles of permittivity ε_2 ($\sim$2).

Combining all the terms leads to a solution for the overall permittivity of the system, $\varepsilon_{eff}(\omega)$:

$$\varepsilon_{eff}(\omega) = \varepsilon_{LF}(\omega) + \frac{G_H}{1 + i\omega\tau_H} + \varepsilon_{wp} + \varepsilon_\infty, \qquad (28)$$

where $\varepsilon_{LF}(\omega)$ represents the low frequency contribution calculated using equations (21) and (22). ε_∞ accounts for the permittivity at higher frequencies beyond the relaxation frequency of water, where the permittivity decreases to a constant value ($\sim$4.5 at 20°C in the case of pure water [10]).

3. Experimental details

The charged colloids consisted of polystyrene particles with surface charge resulting from sulfate surface groups suspended in pure distilled water at a volume fraction of 0.1. The particle diameter, d, varied from 20 to 220 nm.

Measurements of the permittivity of the colloids were carried out using two different experimental techniques in order to cover a broad frequency range. The high frequency measurements (0.1–20 GHz) were carried out using the dielectric probe technique [13]. Here, a Hewlett Packard (HP) 85070A dielectric probe kit was used with a HP 8720B Vector Network Analyser. The complex reflection coefficient of the samples measured using the technique was then converted to the complex permittivity using HP dielectric probe software. The low frequency measurements (1 MHz–1.8 GHz) were carried out using the broadband Novocontrol Spectrometer [14], with a HP 4291 Vector Network Analyser, which used a coaxial line reflection technique. The set-up used parallel electrodes, between which each of the colloidal samples was placed. This allowed the complex capacitance of each of the samples to be measured, from which the resulting complex permittivity was determined. The Win-DETA software package [14] was used to carry out the measurements and evaluate the results.

4. Results and predictions

4.1. High frequency dielectric probe results

Figures 2 and 3 show the high frequency results obtained from the dielectric probe measurements from 0.13 to 20 GHz. The results obtained for water have also been included for comparison.

As shown in figures 2 and 3, the colloids exhibited a relaxation beyond 10 GHz, associated with the dipolar relaxation of water. The permittivity exhibited by the colloids over this region is slightly lower than that produced by pure water due to the presence of the polystyrene particles, which can be predicted from effective medium theories (equation (26)), as demonstrated in section 4.3.

At lower frequencies, water exhibits no relaxation and therefore has a constant real permittivity of 78 and negligible contribution to loss (ε''). However, the colloids show significant particle size-related dispersion, where both the real and imaginary components of permittivity increase as particle size decreases. Significantly, the results show that

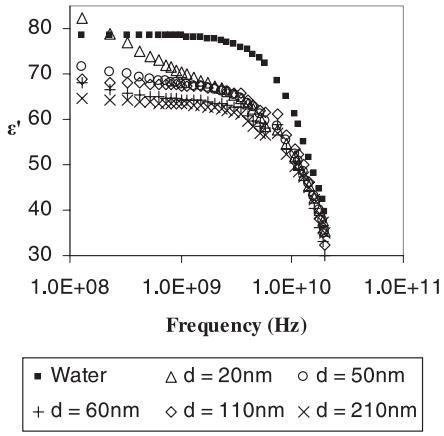

Figure 2. Real permittivity of charged polystyrene colloids at a volume fraction of 0.1 from 0.13 to 20 GHz.

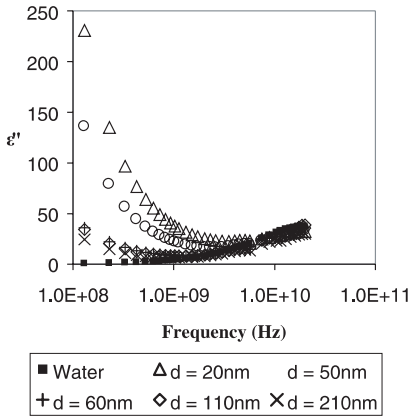

Figure 3. Imaginary permittivity of charged polystyrene colloids at a volume fraction of 0.1 from 0.13 to 20 GHz.

the dispersion extends into microwave frequencies. Although the permittivity is low in comparison with that expected at lower frequencies (section 4.2), the values produced in the microwave frequency region show a relatively high level of loss in comparison with many conventional metal particulate-based composite materials, such as metallic colloids, at the same volume fraction [15]. The ability to increase the level of loss is advantageous in many electromagnetic applications, such as shielding, because it leads to a greater level of absorption. The corresponding loss tangents, $\tan\delta$ ($\varepsilon''/\varepsilon'$) (shown in figure 4) also show significantly high values, reaching loss tangents of up to 3 in the case of the smallest particle colloids (particle diameter of 20 nm) at lower frequencies. The particle size again provides an effective means to control the loss tangents, which are also higher and therefore potentially more beneficial than those expected in many conventional metal particulate-based colloids at the same volume fraction. These can typically be expected to exhibit loss tangents below 1 at these frequencies.

4.2. Low frequency Novocontrol results

Figures 5 and 6 show the combined high frequency dielectric probe and low frequency Novocontrol results to give an overall frequency range of 1 MHz–20 GHz. The two measurement techniques show good agreement with the permittivity

exhibited at radio frequencies substantially higher than that at microwave frequencies. The results again show particle size-related permittivity, which can be optimized over radio and microwave frequencies. Despite the broad frequency range covered, the results do not show any clear peaks associated with either the low or high frequency relaxation regions. The results are discussed further in section 4.3, where they are fitted to a model, which accounts for the three relaxation regions and can be used to determine the origin of the results.

4.3. Comparison between predicted and experimental results

Prediction of the measured imaginary component of permittivity, $\varepsilon''_{\text{eff}}$, includes an additional conductivity contribution, associated with the dc static conductivity, σ_{dc}, of the colloid [19] (as shown in equation (29)) (figure 6):

$$\varepsilon''_{\text{eff}} = \varepsilon''_{\text{ac}} + \frac{\sigma_{\text{dc}}}{\omega\varepsilon_0} \tag{29}$$

with the corresponding ac conductivity, σ_{ac}, given by

$$\sigma_{\text{ac}} = \omega\varepsilon_0\varepsilon''_{\text{eff}} = \omega\varepsilon_0\varepsilon''_{\text{ac}} + \sigma_{\text{dc}}, \tag{30}$$

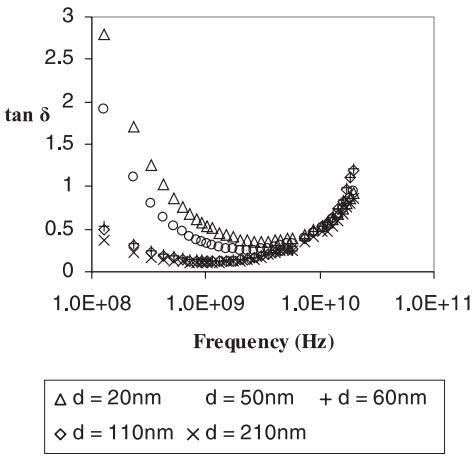

Figure 4. Loss tangent of charged polystyrene colloids at a volume fraction of 0.1 from 0.13 to 20 GHz.

where $\varepsilon''_{\text{ac}}$ represents the imaginary component of permittivity with the dc conductivity removed.

Figure 7 demonstrates the use of the model in predicting the permittivity, $\varepsilon_{\text{eff}}(\omega)$, achievable in a suspension of 100 nm polystyrene particles at a particle volume fraction of 0.1 in water, as highlighted by equation (28). The ac conductivity-related imaginary component of permittivity, $\varepsilon''_{\text{ac}}$, is used here to highlight the different contributions made to the model, which lead to the different loss peaks associated with each relaxation process.

As shown in figure 7, at low frequencies, the overall permittivity response, $\varepsilon''_{\text{ac}}$, is dominated by the low frequency relaxation mechanism. This contribution is accounted for by the model of Chassagne and Bedeaux $\varepsilon''_{\text{LF}}(\omega)$ (as shown by equation (22)). As highlighted in section 2.1, the low frequency relaxation mechanism occurs due to the diffusive motion of ions in the bulk electrolyte, which result from changes in the dipole strength of the double layer due to an applied field. At higher frequencies, the model of Chassagne and Bedeaux produces a negligible contribution and as mentioned in section 2.1, does not account for the permittivity of water or the dipolar relaxation exhibited by it. Here, the high frequency relaxation contribution associated with the tangential and perpendicular flow of counterions in the double layer is accounted for by the Maxwell–Wagner relaxation, $\varepsilon''_{\text{HF}}(\omega)$ (using equations (23) and (24)), where the amplitude increases as surface conductivity increases. As highlighted in section 2.1, the Maxwell–Wagner equation approximates the double layer to a thin conducting shell, with the resulting contribution to interfacial polarization leading to the small amplitude relaxation peak shown in figure 7. A relatively high surface conductivity ($\sigma_{\text{s}} = 2 \times 10^{-8}$ S) is assumed, resulting from a high zeta potential ($\xi = 150$ mV) and a value of $\kappa r = 20$, which are used here to produce an easily distinguishable peak and demonstrate the potential contributions made to the model. A more thorough discussion of the parameters used to model the actual results is given below. A third peak is demonstrated at frequencies beyond 10 GHz, associated with the dipolar

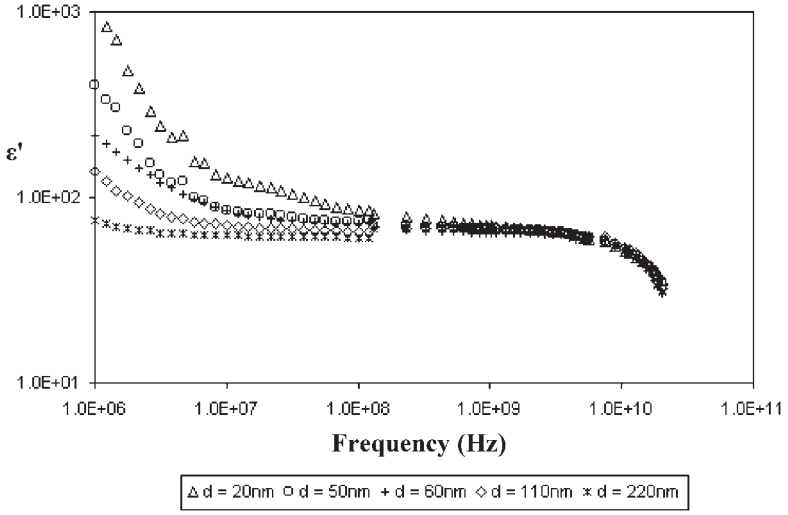

Figure 5. Real permittivity of charged polystyrene colloids at a volume fraction of 0.1 from 10^6 Hz to 20 GHz.

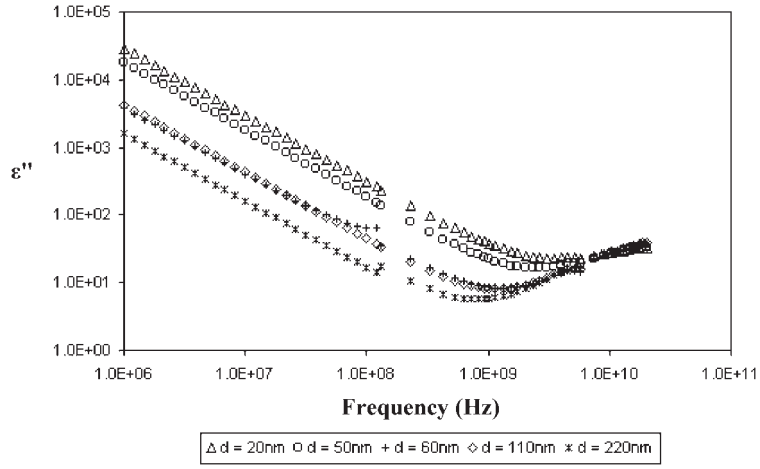

Figure 6. Imaginary permittivity of charged polystyrene colloids at a volume fraction of 0.1 from 10^6 Hz to 20 GHz.

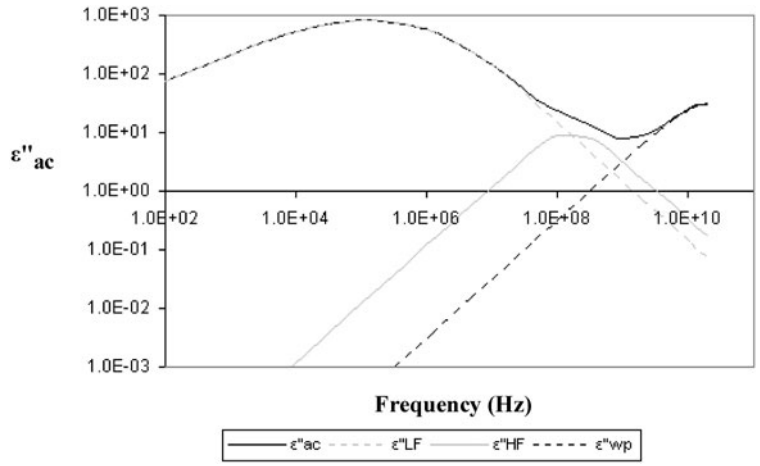

Figure 7. Predicted contributions to the overall imaginary permittivity, ε''_{ac}, of a charged colloid containing 100 nm diameter polystyrene particles at a volume fraction of 0.1.

relaxation (equation (26)) that occurs due to the reorientational polarization that water undergoes. The level of loss at this peak is reduced from that of pure water due to the presence of 10% polystyrene particles as predicted by the Looyenga equation (27).

Figure 8 shows a comparison between the predicted and experimental results for the real permittivity of the charged colloids at four different particle sizes, ranging from particle diameters of 20–220 nm. The performance was modelled using the zeta potential, ξ, and double layer thickness, κ^{-1}, as fitting parameters. A zeta potential of $\xi = 4kT/e$ ($\sim$100 mV) and a value of $\kappa r = 30$ were shown to produce the best fit. These were also similar to values estimated from static conductivity measurements on the colloids using equations given in [9, 16]. Previous research [7, 16–18] into similar particle systems shows that these are realistic estimates, with the zeta potential typically ranging from $\xi = 1kT/e$ to $\xi = 10kT/e$. The double layer thickness is assumed to be thin (i.e. $\kappa r \gg 1$) and so is modelled as a thin conducting shell [7] to provide the high frequency Maxwell–Wagner contribution (equations (23) and (24)).

As shown in figure 8, the experimental results are in good agreement with the predicted results. The largest variation from predicted results occurs for the 20 nm particle colloids. However, there are a number of potential contributions that can account for this relatively small difference such as, experimental uncertainties, a spread in particle size and slight differences in the zeta potential and double layer thickness from the predicted values used.

The modelled results are extended to lower frequencies in figure 8 to demonstrate the origin of the dispersion shown in the results. The comparison shows that the high permittivity values exhibited by the results are due to the low frequency relaxation region, which accounts for the observed dispersion in permittivity with particle size. The predictions for a micron-sized particle have also been included for comparison. As shown, the nanoparticle size leads to a significantly higher relaxation frequency than the micron particle size, which is why the dispersion extends to microwave frequencies for the nanoparticle colloids investigated. The inset figure also shows that the dispersion seen in the low frequency region of the dielectric probe results ($\sim 10^8$ GHz) was due to the low frequency relaxation mechanism, which is consistent with the observed increase in permittivity with decreasing particle size at this frequency region. The inset figure also shows that the

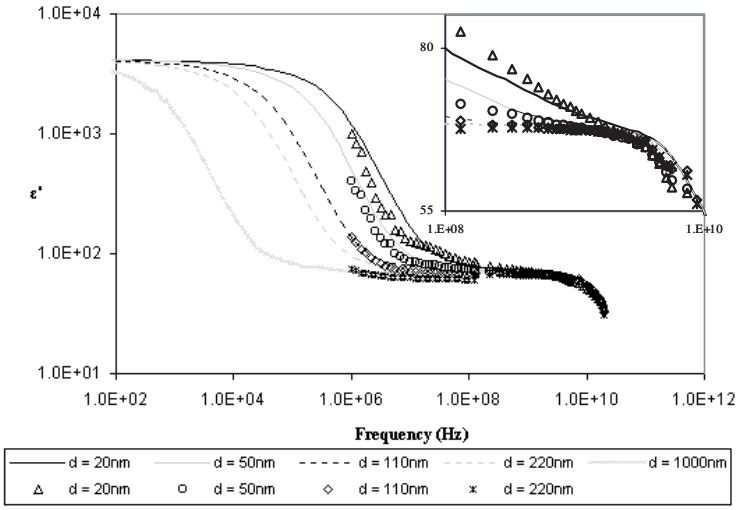

Figure 8. Comparison between predicted and experimental results for the real permittivity of charged polystyrene colloids at a volume fraction of 0.1. The data points correspond to experimental results, and the fitted lines correspond to predictions.

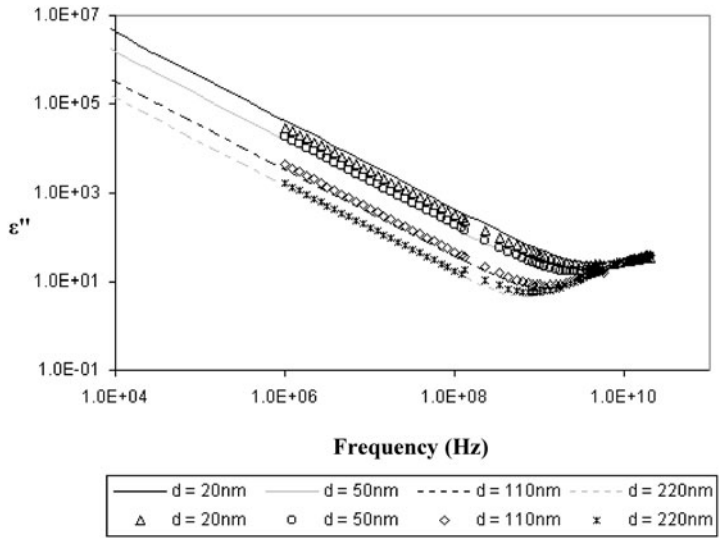

Figure 9. Comparison between predicted and experimental results for the imaginary permittivity of charged polystyrene colloids at a volume fraction of 0.1. The data points correspond to experimental results, and the fitted lines correspond to predictions.

Looyenga equation (27) provides a good approximation of the permittivity response of the colloids at higher frequencies, with the dipolar relaxation apparent in both and occurring in the position predicted by equation (25).

As shown in figure 7, a small amplitude, high frequency relaxation was also expected at frequencies close to the microwave region ($\sim 10^8$ GHz). However, this region is not apparent in the results (shown in figures 5 and 8). This may be because it is relatively small in comparison with the low frequency, high amplitude relaxation, which makes it challenging to detect the above experimental uncertainties. This is also confirmed by the predictions, where the parameters used to model the experimental performance produce a negligibly small contribution in comparison with the low frequency, high amplitude relaxation. In addition to this, the high frequency relaxation region is located close to frequencies where the two sets of experimental measurements meet (i.e. towards the high frequency limit of the Novocontrol set-up and the low frequency limit of the dielectric probe set-up). This adds to the experimental uncertainty when measuring small perturbations. However, the high frequency contribution has also been included in the model because it is potentially an important region for use in microwave applications and its optimization could therefore prove beneficial in such systems. For example (as demonstrated in figure 7), an increase in surface conductivity could lead to a significant increase in amplitude of this high frequency relaxation peak.

Figure 9 shows a comparison between the predicted and experimental results for the imaginary permittivity, $\varepsilon''_{\text{eff}}$, of the charged colloids for the same four particle sizes compared in figure 8, with the same fitting parameters.

The results show agreement with the predictions across the frequency range, with the relatively small variation again accounted for by the factors highlighted in figure 8. As shown, at low frequencies, the dc conductivity tends to dominate the experimentally observed imaginary permittivity.

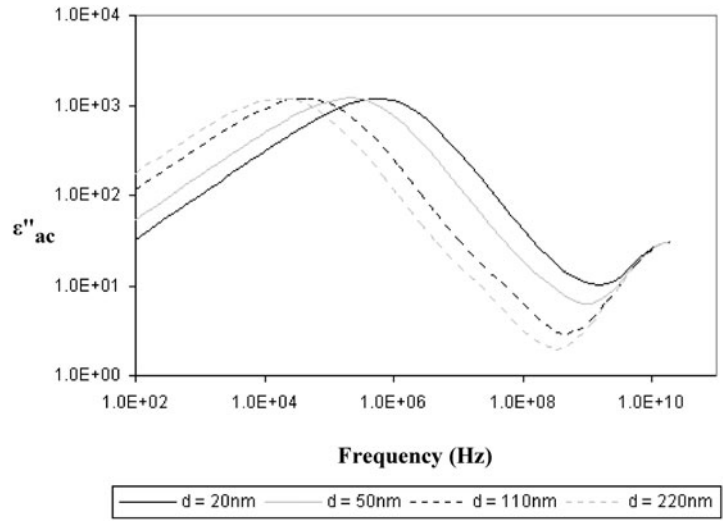

Figure 10. Predicted imaginary permittivity, ε''_{ac}, for results shown in figure 9, with dc conductivity component removed.

Figure 10 shows the predicted imaginary permittivity, ε''_{ac}, at different particle sizes. The figure has been included to demonstrate the relaxation behaviour of the underlying ac conductivity-related imaginary component of permittivity, not observable experimentally because of the dc conductivity contribution.

As shown, a particle size-related imaginary component can again be expected, which increases in frequency as particle size decreases and is consistent with the behaviour of the real component in figure 8. Figure 10 again shows that the dispersion associated with the smaller nanoparticle colloids extends to microwave frequencies.

5. Conclusions

We have investigated the dielectric properties of charged nanoparticle colloids across a range of radio and microwave frequencies. The colloids, which varied from 20 to 220 nm in diameter, were measured using two different experimental set-ups to cover the broad frequency range of 1 MHz to 20 GHz.

The results show that significant permittivity is achievable across radio and microwave frequencies using charged nanoparticle colloids. The results were fitted to a model, which used the zeta potential and double layer thickness as fitting parameters for the low frequency response [5], with the high frequency relaxation and response of water modelled as Debye type relaxations [11]. The model provided good agreement with the experimental performance. Comparison between predicted and experimental results shows that the dispersion produced by the colloids occurs as a result of the low frequency relaxation, which can be tuned across a range of frequencies through particle size. This research has shown that the small nanoparticle sizes investigated lead to faster relaxation times than those expected from conventional micron sized particles, such that the control of the dielectric properties can be extended into the microwave region to provide significant levels of loss.

The parameters used to model the experimental performance show that the high frequency relaxation produces a negligibly small contribution, in comparison with the low frequency high amplitude relaxation. Because of the high frequency position of this peak, it is potentially an important region for use in microwave applications and its optimization could therefore prove beneficial in such systems. For example, increasing the surface conductivity through the zeta potential could result in a higher amplitude relaxation peak related to the Maxwell–Wagner process.

Acknowledgments

The authors acknowledge the funding of this research by the Ministry of Defence via the Applied Research Programme.

References

[1] Lyklema J and Van Leeuwen H P 1999 *Adv. Colloid Interface Sci.* **83** 33
[2] O'Konski C T 1960 *J. Phys. Chem.* **64** 605
[3] Schurr J M 1964 *J. Phys. Chem.* **68** 2407
[4] Hinch J E 1984 *J. Chem. Soc. Faraday Trans.* II **80** 535
[5] Chassagne C and Bedeaux D 2001 *J. Phys. Chem.* **105** 11743
[6] O'Brien R W 1986 *J. Colloid Interface Sci.* **113** 81
[7] Grosse C and Tirado M 1998 *J. Colloid Interface Sci.* **205** 26
[8] Russel W B and Saville D A 1989 *Colloidal Dispersions* (Cambridge: Cambridge University Press)
[9] Hunter R J 1992 *Foundations of Colloid Science* (Oxford: Oxford University Press)
[10] Craig D Q M 1995 *Dielectric Analysis of Pharmaceutical Systems* (London: Taylor and Francis)
[11] Grosse C and Barchini R 1986 *J. Phys. D: Appl. Phys.* **19** 1957
[12] Choy T C 1999 *Effective Medium Theory: Principles and Applications* (New York: Oxford University Press)
[13] Agilent web site: www.agilent.co.uk
[14] Novocontrol web site: www.novocontrol.com
[15] Nimtz G and Enders A 1992 *Int. J. Electron.* **73** 983
[16] Grosse C 1988 *J. Phys. Chem.* **92** 3910
[17] Emma H and Delacey B 1981 *J. Chem. Soc. Faraday Trans.* II **77** 2007
[18] Mangelsdorf C S and White L R 1997 *J. Chem. Soc. Faraday Trans.* **93** 3145
[19] Lian A and Besner S 1995 *Synth. Met.* **74** 21